

# Influence of Form and Structural Features of Open-Cell Hybrid Foam on the Remanent Magnetic Scanning

Bashar Ibrahim,\* Michael M. Becker, Francesco Kunz, Anne Jung,  
and Sarah C. L. Fischer\*

Hybrid foams are promising materials for a wide range of applications due to their high strength and low weight. Due to the manufacturing process, the material properties are heterogeneous, therefore requiring characterization methods to quantify local coating layer thicknesses for both research and process scale-up. Compared to microscopy, remanent magnetic scanning enables shorter turnaround times for the estimation of coating thickness. This study aims to improve quantitative characterization with magnetic scanning measurements by proposing an equivalent model for open-cell hybrid foams. This model helps to identify possible sources of deviations in the thickness-magnetic correlation that can occur in hybrid foams. Simulations reveal that several geometrical features contribute ambiguously to the magnetic field. The level of influence on the magnetic signal varies depending on the feature under investigation and its proximity to the surface. High influence is observed for displaced cells in the depth and vertical struts at varying depths compared to adjacent cells on the surface. This should be considered when using remanent magnetic scanning for the quantitative estimation of local coating thickness. In the future, more experimental data may help to use this approach for quantitative characterization of layer thicknesses and reduce ambiguity of the measured data.

These foams mimic the microstructure of natural materials like trabecular bone<sup>[3]</sup> and have a wide range of applications, including heat exchangers, catalytic coatings, electrodes in batteries, and fuel cells. Moreover, they are also used as lightweight construction materials in industries such as automotive, aerospace, and building protection, providing a cost- and resource-efficient alternative to traditional materials.<sup>[3–8]</sup> Open-porous metal foams also have potential applications in energy absorption and mechanical damping.<sup>[7,9]</sup> While aluminum foams have been commonly used in the past, their production is very expensive, complex, and not always reproducible because of casting inhomogeneities.<sup>[10]</sup> To create new hybrid materials, different components with varying properties are combined to meet multiple specifications simultaneously. By combining cost-efficient polyurethane (PU) foam with a thin coating of mostly nanocrystalline metal, the low-cost template structure is significantly reinforced in terms of mechanical stiffness and

reproducibility. The coating of the open porous foams can be achieved by various methods,<sup>[8]</sup> but the galvanic deposition in particular offers a wide range of controllable parameters for industrial production. The specific energy absorption capacity of the developed hybrid foams increases significantly with a 150 micro meter thick layer of nanocrystalline nickel (Ni), compared to, for example, regular metallic (Al) foams.<sup>[10,11]</sup> The increased stiffness improves compressibility, making hybrid foams suitable for damping and energy absorption applications, especially in automotive industry and protective systems. The reason for their excellent energy absorption capacity is given by the microplasticity of their struts, which are stochastically distributed in the open porous foam. Layerwise compression of the different pore layers within the foam volume increases the dissipation of the mechanical energy during the crash event.<sup>[12]</sup>

The thickness of the nickel coating is an important parameter affecting the mechanical behavior of these materials. The variation of the coating during the manufacturing process requires a continuous investigation of the local coating thickness along the sample surface and at varying depths.<sup>[13]</sup> For studying the thickness and the distribution of the coating layer, a 3D finite element simulation is required. Using fully resolved, real-world geometry model of open-cell foams presents several challenges, such as


## 1. Introduction

Low density and high surface-to-volume ratio have made open-porous metal foams increasingly popular in recent years.<sup>[1,2]</sup>

B. Ibrahim, M. M. Becker, S. C. L. Fischer  
Fraunhofer Institute for Nondestructive Testing  
IZFP

Campus E3 1, 66123 Saarbrücken, Germany  
E-mail: bashar.ibrahim@izfp.fraunhofer.de;  
sarah.fischer@izfp.fraunhofer.de

F. Kunz, A. Jung  
Protective Systems  
Helmut-Schmidt-University/University of the Federal Armed Forces  
Hamburg  
Holstenhofweg 85, 22043 Hamburg, Germany

 The ORCID identification number(s) for the author(s) of this article can be found under <https://doi.org/10.1002/adem.202402034>.

© 2025 The Author(s). Advanced Engineering Materials published by Wiley-VCH GmbH. This is an open access article under the terms of the Creative Commons Attribution License, which permits use, distribution and reproduction in any medium, provided the original work is properly cited.

DOI: 10.1002/adem.202402034

creating and connecting mesh elements on strut-coated surfaces. In many works,<sup>[14,15]</sup> the high-resolution 3D voxel data was used to build a numerical model of a small volume cell. This resulted in a large number of degrees of freedom. Furthermore, this number increases rapidly when modeling the entire sample volume instead of using a single-cell model.

The discretization of the model using finite cell method (FCM) significantly reduces the computation time for voxel models obtained from CT scans. However, it is not possible to change the model geometry to study new samples with these models. The heterogeneous nature of the open-cell foam requires an automated model that can adapt to any geometry deviation in the subsequently manufactured samples.

Kunz et al.<sup>[13]</sup> introduced a simplified numerical model that allowed the representation of the magnetic properties of the nickel-coated open-cell foams without the need to explicitly model the complex geometrical features of the samples. The simulation results confirmed a possible qualitative estimation of the coating thickness using the remanent magnetic field scanning. However, some discrepancies were found when comparing the magnetic curve from the simulation and the experimental data. Building on our previous work, the present study discusses possible reasons for this deviation by iteratively integrating the structural and morphological features of an open-cell sample into the simplified model and analyzing their effect on the magnetic signal by comparing the simulation data with the experimental measurements. Therefore, in this study, an equivalent model of a hybrid foam is constructed by replacing the ferromagnetic nickel-coated foams with a set of geometrically predefined permanent magnets. In addition, the pores between the struts are replaced with air gaps in the model. Round surfaces and edges are avoided by the choice of magnet geometry, as these geometries increase the number of mesh elements and thus the computation time. A better understanding of the effect of the hybrid foam geometrical features on the measured magnetic signal is sought, taking into account their proximity to the evaluation line and the scanned cells. Each feature is integrated separately into the simplified model, and the simulation results are examined.

## 2. Experimental Section

### 2.1. Hybrid Foam Samples

The investigated open-cell hybrid foam samples consists of a series of structural elements referred to as struts.<sup>[16]</sup> These struts

forms together the cells that contain the pores. The hybrid foam struts, as illustrated in **Figure 1a**, have a random orientation in the sample, resulting in a stochastic cell and pore size in the three spatial dimensions. The pore size is also influenced by the coating process, which in some cases can close the pores completely (see **Figure 1a**). The coating thickness varies along the sample as shown in **Figure 1b** and can be estimated using the remanent magnetic scanning method.<sup>[17]</sup>

The wide range of morphological features in the open-cell foam samples led to the adoption of an equivalent numerical model, referred to as the simplified model.<sup>[17]</sup> The main objective of this study is to investigate the possibility of detecting various effects of the hybrid foam geometry in the measured signal and isolating them from signal information related to coating thickness variations.

### 2.2. Simplified Simulation Model

The model used in this simulation is constructed from a set of parametric rectangular cuboid permanent magnets separated by air gaps. The air gaps represent coating discontinuities and voids between the struts. The cuboid magnets represent the nickel-coated struts, which have ferromagnetic properties. The height of the magnets in the model is dependent on the thickness gradient from optical measurements of open-cell samples (see **Figure 3** and **Table 3**). The magnets are modeled in Comsol software (version 5.6) using its geometry tool, which allows a flexible adjustment of the cuboid dimensions, orientation and positions. To study the influence of the selected features of the hybrid foams, the magnets size, orientation, and position are varied successively as shown in the results section. The parameterization for the dimensions are given in the respective sections.

### 2.3. Modeling

The Magnetic Fields, No Currents physic (AC/DC) in Comsol is selected in the simulation as it is normally used for the calculation of static magnetic fields such as those generated by the magnetized nickel layer.<sup>[18]</sup> The magnetic field is calculated by solving Gauss's law using the scalar magnetic potential  $V_m$ .

To study the features influencing the measurement signal in the method described in ref. [17] the magnetization field with an intensity of  $10 \text{ kA m}^{-1}$  is chosen to have only a vertical component. Depending on the type of simulation, the magnetization vector can be described as follows.

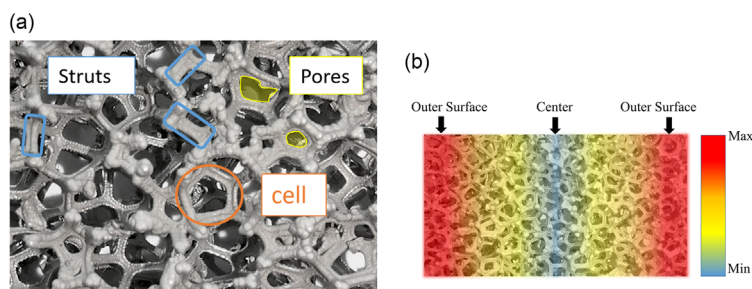


**Figure 1.** Morphology of a hybrid foam. a) Optical micrograph of the structure of an open-cell foam and its components. b) Schematic representation of the coating thickness variation from sample outer surface to its center.

$$M_y = \begin{pmatrix} 0 \\ 10 \end{pmatrix} \quad (1)$$

$$M_z = \begin{pmatrix} 0 \\ 0 \\ 10 \end{pmatrix} \quad (2)$$

where the value in Equation (1) is for the case of 2D simulation and Equation (2) is for 3D simulation. The magnetic flux density  $B$  can then be calculated using the equation.

$$B = \mu_0(H + M) \quad (3)$$

where  $B$  is the vector magnetic flux density,  $H$  is the vector magnetic field intensity, and  $M$  is the magnetization vector.  $\mu_0$  is the permeability of free space with  $\mu_0 = 4\pi \cdot 10^{-7}$  H/m.

#### 2.4. Simulation Verification

As illustrated in **Figure 2**, the simulation model is constructed with an air domain containing rectangular coil magnets. The exterior boundary of the air domain cube is assigned a magnetic insulation boundary condition. The magnets are set to have a constant thickness of 1 mm. To ensure reliable simulation results, several parameters are iteratively adjusted, including the air domain size, mesh density, grid method or discretization type, and solver settings. This is carried out using a 2D simulation approach due to its lower memory consumption and computation time. Since the static magnetic field is the point of interest, the simulations are performed using a stationary study. The size of air domain is investigated as it directly affects the magnetic field propagation around the magnets.<sup>[19]</sup> For this purpose, a parametric study is performed by varying the edge length of the air cube from 50 to 200 mm. Throughout this study, the mesh size in the air domain is kept constant at 0.5 mm, while in the magnets domain, it is set at 0.02 mm. This ensures that the

mesh does not affect the results and allows a more accurate investigation of the desired parameters. The simulation is repeated using the infinite domain feature, focusing specifically on an air domain with an edge length of 100 mm and a layer thickness of 10 mm. The comparison of simulation results indicates that utilizing the infinite domain feature eases the impact from the air domain size on the results. The solution obtained from the infinite domain function converges to the solution obtained with significantly larger domain sizes, which requires an extensive memory usage and longer computation times. For this reason, the infinite air domain feature is used to study mesh properties, discretization, and their effect on simulation results.<sup>[20]</sup> The triangular mesh size in both the magnets and air domains is set to “physic controlled-fine” and the discretization order is varied from linear to quartic. The magnitude of the magnetic flux density  $B_y$  is evaluated along the model at distances of 1 to 5 mm. Applying a higher degree of discretization than that of a linear level results in the generation of a magnetic curve that is more uniform and smooth. However, once the discretization reaches a quadratic level, the smoothness remains relatively constant despite a significant increase in the computation time.<sup>[21]</sup> Therefore, a quadratic discretization is chosen to study the influence of the mesh on the results. A mesh refinement study is selected separately for the magnet and air domains. The study yields the mesh parameters shown in **Table 1** as they provide reliable simulation results. Examining the effect of mesh refinement at higher discretization orders reveals that its influence on improving simulation accuracy is limited.

So far, the out-of-plane thickness in the model has been set to 1 mm, which is applied uniformly to both the magnets and the air domains. Consequently, the propagation of the magnetic field in the 2D simulation is limited in the thickness direction. Since the real magnetic field propagates in the three spatial dimensions, the subsequent simulations are performed in a 3D space using the previously chosen simulation parameters.

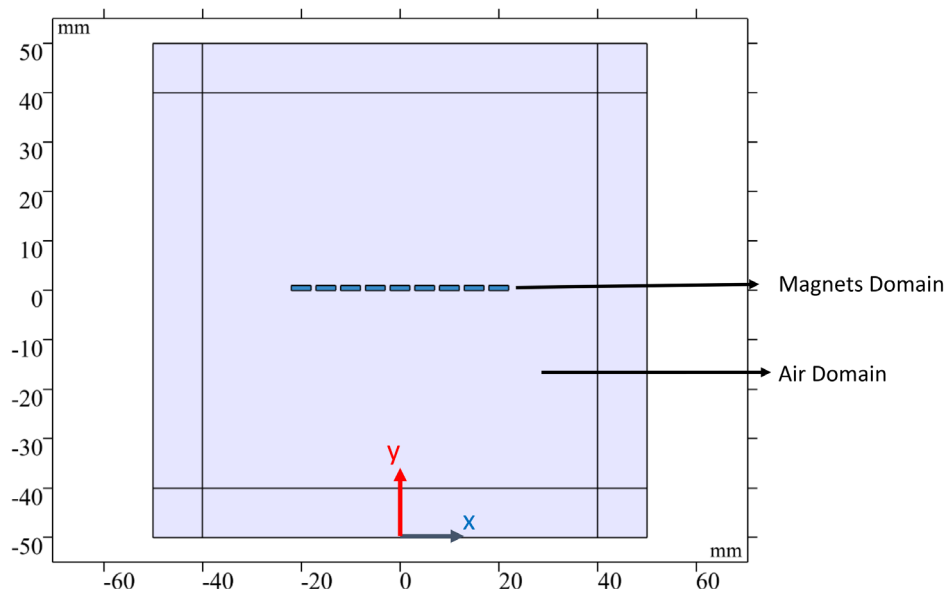


**Figure 2.** 2D model used for verification analysis.

**Table 1.** Mesh parameters for 2D and 3D simulation.

Parameter	2D simulation		3D simulation	
	Magnets domain [mm]	Air domain [mm]	Magnets domain [mm]	Air domain [mm]
Maximum element length	0.2	1	0.2	8
Minimum element length	0.0014	0.002	0.2	1
Growth rate	1.1	1.1	1.1	1.45
Curvature factor	0.2	0.2	0.2	0.5
Resolution narrow regions	1	1	1	0.6

The simulations are conducted using a cubic discretization in the 3D model and applying the mesh parameters given in Table 1. This leads to comparable results as those achieved with higher discretization level and reduces computation time.

Solver settings are examined and adjusted to achieve a balance between accuracy and computation time.<sup>[22,23]</sup> The direct solver (PARDISO) reaches a converged solution in 1 minute and 9 seconds. The iterative multigrid solver takes 2 minutes and 13 seconds to reach convergence and delivers highly comparable results. Therefore, the direct solver (PARDISO) is used in the following simulations due to its efficiency and ability to provide accurate results in a shorter computation time.

### 3. Influencing Features

Several geometrical features influence the mechanical magnetic behavior of hybrid foams such as pores anisotropy, coating thickness and struts dimension and alignment.<sup>[16,24–26]</sup> Other geometrical features such as strut curvature, foam topology, and foam node rounding are mentioned and studied in ref. [26] As the goal of this investigation is to model the magnetic measurements of hybrid foam coating thickness, the simplified model presented in this work does not cover all the morphological features but focuses on those that are conjectured to influence the magnetic signal. Some of these features, shown in **Figure 3**, are as follows: strut dimensions, which is studied by varying the width of the magnets; adjacent cell, which is studied with two sets of magnets, either next to each other or stacked; coating discontinuity, which is studied by varying the gap distance between magnets; tilt angle of struts and cell size variation, which is studied by modifying the tilt angle of the magnets; the alignment of struts on the surface; and vertical struts in the depth.

The hybrid foam morphological features impact on the signal is studied by analyzing the difference between simulation and measurement results. The difference is defined by a deviation area between the simulation and measurement signal curves (see **Figure 4**). It can be observed that the variation in the measurement curve along the measurement line is less than that of the simulation curve. The simulation curve demonstrates a repetitive pattern of maximum and minimum peaks. Both curves are normalized to their maximum value and studied around these peaks (a and b regions). The center of these regions corresponds

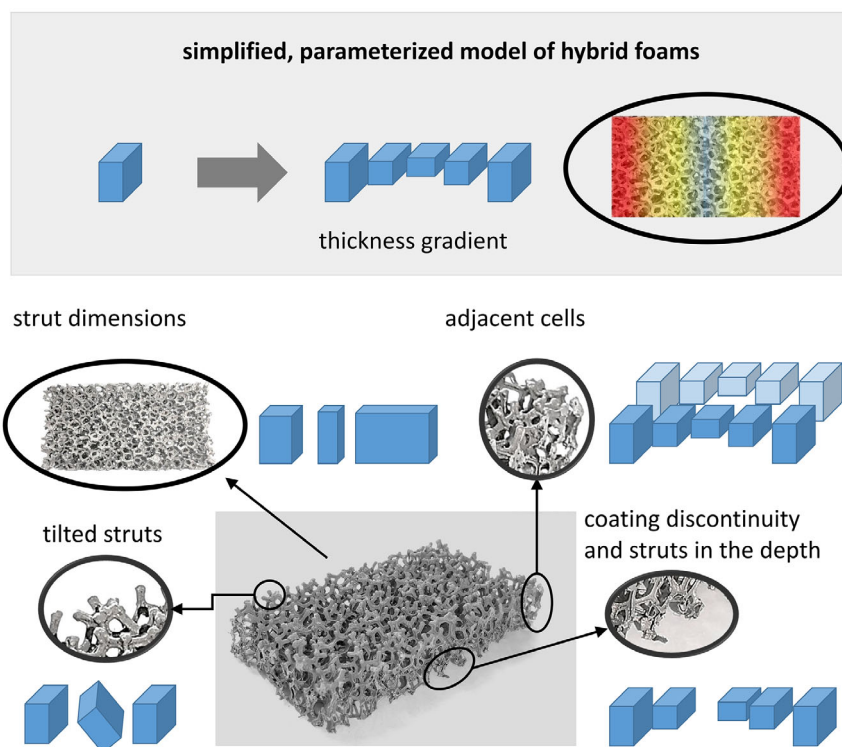


**Figure 3.** Selected geometrical features of the open-cell foam sample from ref. [17] and their representation in the simplified model for analyzing their influence on the magnetic measurement signal.

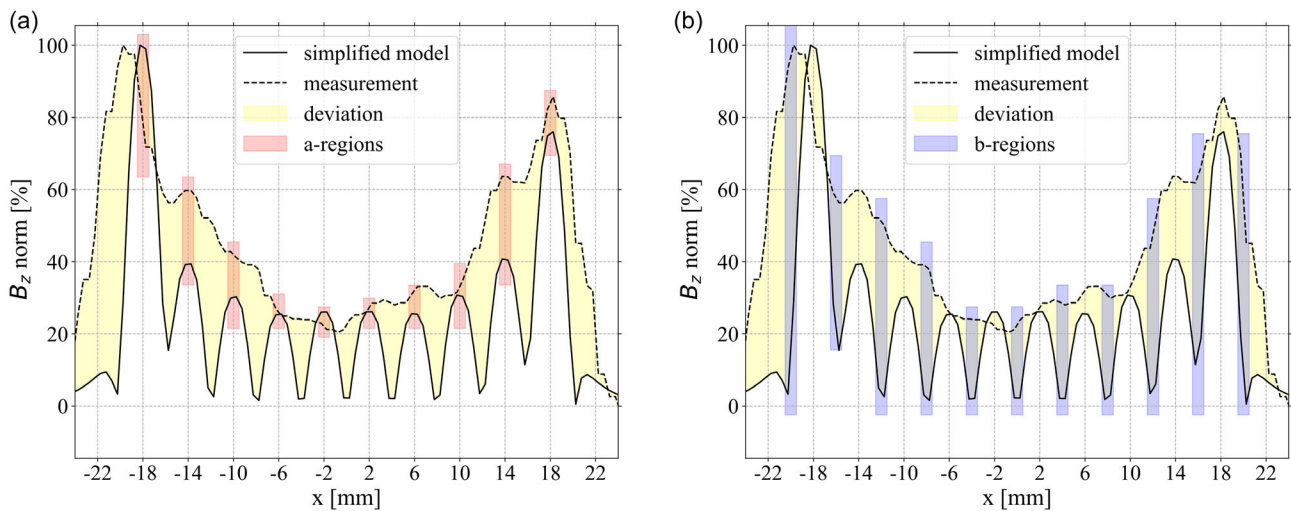


**Figure 4.** Magnetic field curve from the simulation of the simplified model compared to measured values from the remanent magnetic scanning. Both simulation and measured values are normalized to their maximum. a) The simulation and magnetic curves with the highlighted a regions. b) The curves with the highlighted b regions.

to the maxima of the simulation curve for a regions and the minima for b regions. The width of both regions is set to 1 mm. Within these regions, the average of each curve is calculated and compared to the average of the other curve. The resulting curve from each feature and its deviation from the measurement is compared to the simplified model curve deviation.

### 3.1. Strut Dimensions

In this section, the influence of strut dimensions will be studied. The model utilized represents a single measurement along the sample length. Consequently, only struts situated along the designated measurement line, which is set to 44 mm, are modeled. This means that struts from neighboring regions on the surface and in the depth are not represented in the initial simulation model. Moreover, the modeled struts are assumed to have a uniform length, width, orientation, and tilt angle (see Figure 3).

The coating thickness gradient is accounted for in the numeric model by changing the height of the magnets  $H$  (as illustrated in Table 2). The coordinate  $x$  refers to the center of the magnets in the numerical model, where the evaluated  $z$ -component of the magnetic flux density  $B_z$  is at its maximum.

The effect of strut dimensions on the correlation is investigated by applying a parametric study to the model. In this study, the width of the magnets is varied from 0.5 to 10 mm, and thickness is assumed to be equal to the height of the magnets, as shown in Table 2. The magnetic flux density is evaluated at 1 mm from the model surface parallel to the symmetry line of the magnets where  $y=0$  (red line in Figure 5c). An additional

**Table 2.** Variation of magnet height  $H$  in the simulation at specific points  $x$  along the evaluation line.

$x$ [mm]	-20	-15	-10	-5	0	5	10	15	20
$H$ [ $\mu\text{m}$ ]	1000	400	300	250	200	250	300	350	700

evaluation is then carried out parallel to the edge of the magnets at the same distance (orange line in Figure 5c). Both evaluation lines have the same length. By comparing the results of the two evaluation lines, the effect of the measurement position on the correlation can be examined. Both the calculated magnetic flux  $B_z$  and the thickness profile  $T$  are normalized to their respective maximum values for an efficient analysis and ease of observations. The normalization is particularly valuable when comparing results obtained at significantly different evaluation distances, as the magnetic flux is inversely proportional to the distance from magnetic field source.

As illustrated in Figure 6a, the simulation results indicate a specific magnets dimension at which the correlation between coating thickness and magnetic flux is at its maximum. For the selected magnet length of 4 mm, the highest correlation is observed around a width of 5 mm when the evaluation is selected in the symmetry plane of the magnets. When the evaluation line is shifted to be along the edge of the magnets, a reduced correlation is observed for the width of 5 mm, resulting in a decrease in the accuracy of the thickness estimation. The estimation error in this case is relatively low for a width of 3 mm. Since the orientation, length, and width of the struts vary along the surface of the sample, the measurement line will experience a continuous transition from the symmetry line to the edge line, and thus, the correlation value will fluctuate depending on the value of the measured magnetic flux.

### 3.2. Adjacent Cells

In the following simulations, the evaluation is performed in the symmetry plane in order to obtain the maximum  $B_z$  and a better correlation. The simulation model is modified to match the sample length and thickness measurement points by setting each magnet length to 3 mm and width to 5 mm. The measurement signal is obtained by scanning a hybrid foam sample with the coating thickness  $T$  presented in Table 3 along with the selected magnets height  $H$  in the simulation. The investigated sample

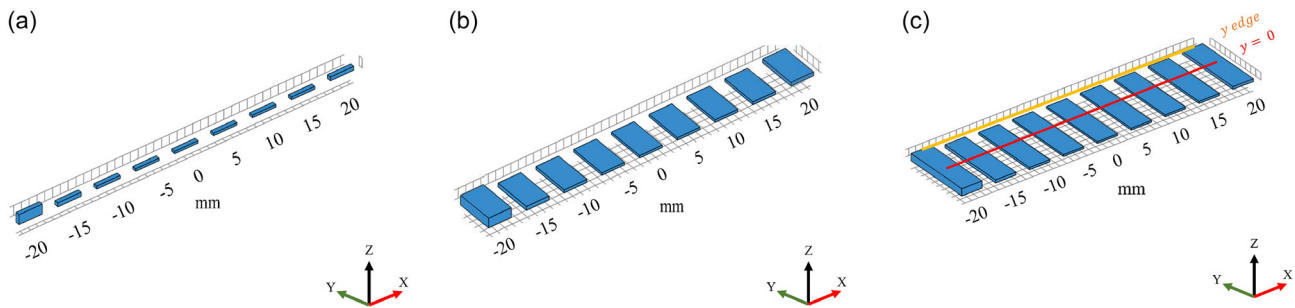


**Figure 5.** Magnet width variation in the simplified model. Depicted are exemplary variations of the width of a) 0.5 mm, b) 5 mm, and c) 10 mm.

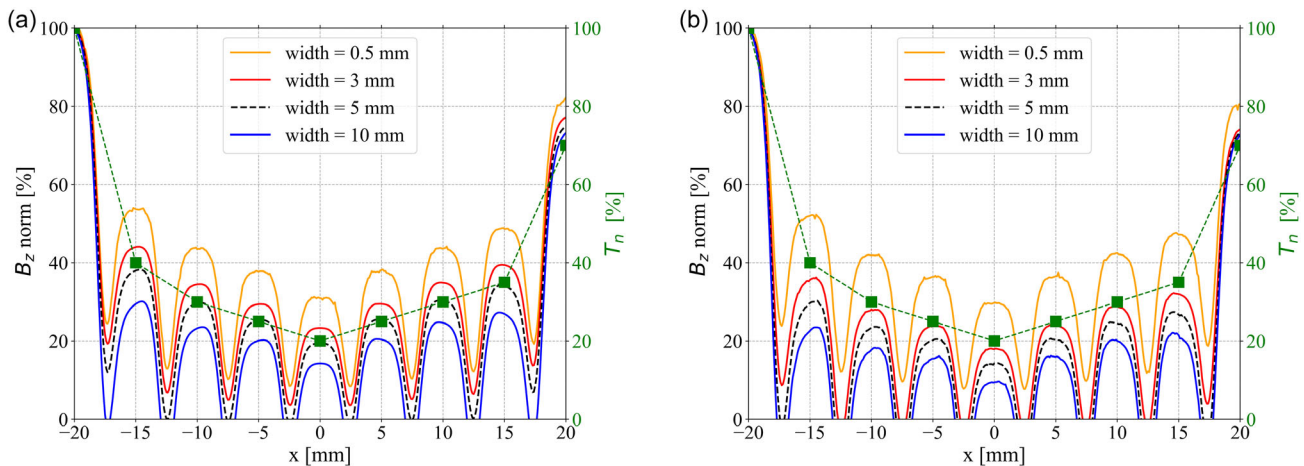


**Figure 6.** Simulation results of models with various magnet widths compared to the coating thickness curve (green line). The evaluation is carried out at a z-distance of 1 mm above the magnet surface. The evaluation is conducted at two different positions: a) along  $y = 0$  and b) along the edge of the magnet.  $T_n$  refers to the coating thickness and  $B_z$  norm the magnetic flux density; both are normalized to their maximum value.

**Table 3.** The measured coating thickness  $T$  and the magnets height  $H$  along the evaluation line.

$x$ [mm]	-18	-14	-10	-6	-2	2	6	10	14	18
$H$ [ $\mu\text{m}$ ]	1000	400	300	250	240	250	260	280	380	700
$T$ [ $\mu\text{m}$ ]	184.02	73.37	56.13	47.53	45.73	45.11	48.36	52.77	70.63	132.42

length is 40 mm, and the pore size is 10 ppi. The model total length is set to start with 39 mm and is varied according to the investigated feature.

The investigation of the influence of adjacent cell struts that are located on the sample surface is achieved by adding an additional set of magnets with the same thickness profile. These magnets are shifted by  $b_{xy}$  distance from the original model along the  $y$ -axis and have the same length, width and height as the original magnets (see **Figure 7a**). The distance between the two sets of magnets  $b_{xy}$  is varied using a parametric study. The purpose of this study is to understand how the proximity of adjacent struts affects the overall measured magnetic flux density. The overlap

between the field lines of neighboring magnets is strongly dependent on the distance between them, since the magnetic flux density is inversely proportional to the distance from the field source.

Adding the second set of magnets results in a decrease in the magnetic flux density. This reduction is primarily related to the common magnetization direction of the magnets, which results in the magnetic fields of the two sets opposing each other at the measurement region. The impact of this set on the deviation from the measurements is illustrated in **Table 4** and **5**. The simulation results indicate a notable decline in the magnetic flux produced by the adjacent struts when the value of  $b_{xy}$  exceeds 5 mm. The impact of the additional magnets results in an enhancement of the correlation between simulation and measurement curves in the vicinity of the model central region  $x = -2$  mm for a regions. In b regions, the additional set leads to reducing the alignment with the measurements, thereby producing a greater deviation as in the simplified model. In a subsequent simulation, a set of magnets is integrated into the simplified model in the depth along the  $z$ -axis with  $b_{xz} = 1$  mm. The thickness of the added magnets is set to the same value as the surface thickness, as the coating process ensures a relatively constant thickness along the sample depth<sup>[13]</sup> and the distance  $b_{xz}$  is varied from 1 to 5 mm. The aligned magnetization direction of both surfaces and depth magnets results in an increase in the evaluated

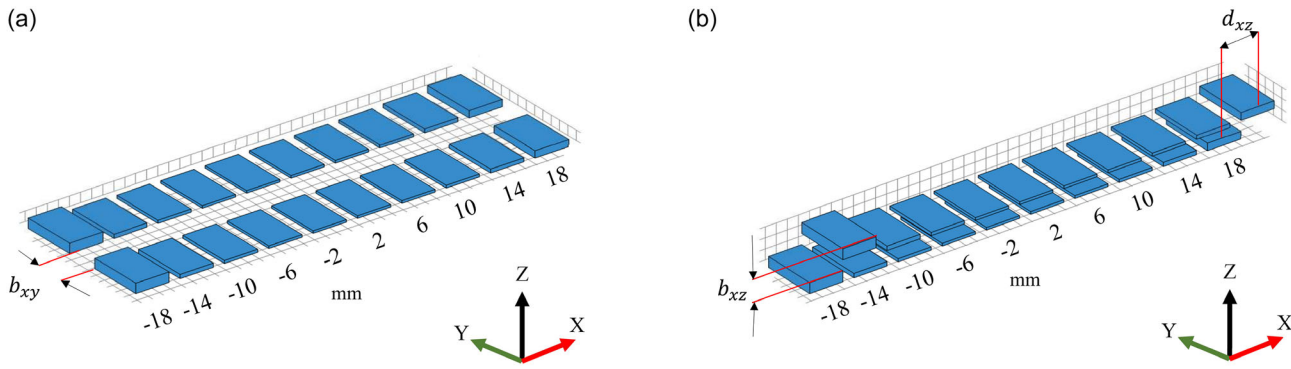


**Figure 7.** Adjacent cells' influence in the simulation model. a) Added set of magnets in the  $xy$ -plane. b) Added set of magnets in the  $xz$ -plane.

**Table 4.** Mean values of magnetic field in the simulation and measurement curve for features in a regions.

Distance [mm]	mean of values of $B_z$ [%] within $x \pm 0.5$ [mm]									
	-18	-14	-10	-6	-2	2	6	10	14	18
	Measurement									
	80.56	59.18	41.78	26.56	22.13	27.19	31.66	33.71	62.71	81.57
	Simplified model									
	95.96	37.91	28.91	24.46	23.88	25.14	25.91	27.13	37.15	73.03
	Adjacent cells on the surface									
$b_{xy}$										
1	95.63	34.18	25.70	21.67	21.20	22.65	23.47	23.96	33.86	72.46
3	95.82	35.96	27.10	22.83	22.25	23.68	24.57	25.27	35.33	72.80
5	95.86	36.76	27.75	23.38	22.74	24.17	25.07	25.86	35.94	72.89
	Adjacent cells in the depth									
$b_{xz}$										
1	96.58	46.02	33.86	28.55	27.56	29.11	30.33	31.48	43.40	76.64
3	96.50	42.85	32.05	26.86	25.89	27.30	28.43	29.83	40.87	74.44
5	96.24	40.92	31.06	26.08	25.16	26.51	27.61	28.89	39.30	73.68
	Adjacent cells in the depth with a displacement									
$dxz$										
1	95.76	48.20	34.33	28.51	27.31	28.80	29.97	30.98	42.18	77.47
3	95.98	58.94	42.71	34.14	31.86	32.90	34.28	35.61	46.16	85.97
5	96.30	60.27	50.70	38.08	34.62	35.25	36.62	38.00	48.44	88.74
	Coating discontinuity									
0.5	97.87	35.61	26.23	22.04	21.48	22.87	23.70	24.38	34.60	73.25
0	98.37	34.96	25.32	21.21	20.70	22.09	22.90	23.53	33.89	73.25
	Tilting in $+45^\circ/-45^\circ$									
	85.67	38.79	27.22	23.00	23.38	23.40	23.19	27.56	38.31	65.60
	Struts alignment on the surface									
$hxz$										
0.1	95.75	42.02	28.34	26.81	24.58	27.53	23.99	32.26	38.46	78.72
0.3	95.49	51.47	26.99	32.40	23.54	33.12	22.87	38.93	36.98	92.18
0.5	85.35	56.08	22.96	34.96	20.05	35.58	19.33	41.95	31.65	96.62
	Vertical struts in the depth									
$rxz$										
1	96.46	41.12	31.22	26.52	27.16	27.46	27.37	33.27	43.36	76.50
0	97.53	40.57	31.02	26.34	27.11	27.39	27.07	33.03	43.24	79.59

magnetic flux within the model. By normalizing this flux to its maximum value, it can be seen that the influence of magnets in the depth decreases for relatively high  $b_{xz}$  values. As illustrated in Table 4, the impact from the magnets in the depth is the lowest

around the middle regions  $x = -2$  mm where the thickness is low and around the left edge of the model  $x = -18$  mm where the thickness is at its maximum. For b regions, the correlation improvement is observed for low  $b_{xz}$  values, with the greatest

**Table 5.** Mean values of magnetic field in the simulation and measurement curve for features in b regions.

Distance [mm]	Mean of values of $B_z$ [%] within $x \pm 0.5$ [mm]										
	-20	-16	-12	-8	-4	0	4	8	12	16	20
	Measurement										
	94.42	58.64	50.34	37.27	24.04	22.61	28.63	31.11	48.98	65.31	59.22
	Simplified model										
	22.71	28.94	8.86	6.54	5.72	5.97	6.39	6.58	8.71	21.32	16.13
	Adjacent cells on the surface										
<i>bxy</i>											
1	21.40	24.34	5.79	5.17	4.76	4.65	4.81	4.90	5.78	17.27	16.79
3	21.71	26.72	6.34	4.74	4.08	4.08	4.31	4.49	6.52	19.21	16.47
5	22.11	27.65	7.28	5.07	4.43	4.74	5.06	5.39	7.62	20.20	16.30
	Adjacent cells in the depth										
<i>bxz</i>											
1	27.23	40.43	17.57	12.99	11.44	11.72	12.37	12.91	16.66	32.14	20.08
3	25.28	35.94	14.82	10.92	9.45	9.71	10.26	10.84	14.12	27.68	18.19
5	24.24	32.79	12.55	9.29	8.10	8.21	8.71	9.24	12.16	24.83	17.16
	Adjacent cells in the depth with displacement										
<i>dxz</i>											
1	23.05	43.80	20.68	14.96	12.91	12.95	13.66	14.38	17.15	32.39	26.67
3	21.33	47.76	28.38	18.65	15.35	14.86	15.61	16.39	18.80	34.13	33.48
5	22.15	35.54	33.99	23.27	17.80	16.36	16.24	17.17	20.07	33.74	32.04
	Coating discontinuity										
0.5	38.19	55.31	23.79	18.80	16.93	17.20	17.99	18.73	23.09	43.55	28.24
0	43.99	65.47	29.58	23.53	21.17	21.51	22.54	23.41	28.62	52.17	32.65
	Tilting in $+45^\circ/-45^\circ$										
	32.04	24.46	20.90	5.09	14.26	4.92	14.29	5.33	22.22	17.80	22.67
	Struts alignment on the surface										
<i>hxz</i>											
0.1	24.37	31.89	10.29	7.60	7.04	7.23	7.02	7.83	11.25	23.98	17.28
0.3	27.30	37.61	13.03	9.77	8.93	9.27	9.00	10.02	13.98	28.70	20.33
0.5	27.75	39.05	14.48	10.71	9.81	10.15	9.81	10.90	15.02	30.08	21.07
	Vertical struts in the depth										
<i>rxz</i>											
1	49.67	40.29	19.32	15.38	14.60	15.26	15.27	16.94	22.61	34.33	32.28
0	88.18	60.52	30.39	24.50	23.39	24.54	25.08	27.25	38.22	49.48	68.33

influence occurring near the edges of the model  $x = 16$  and  $x = -16$  (see Table 5). Given the variability in the dimensions of the sample cells, the strut position in the depth can be adjusted along the  $x$ -axis, relative to the struts on the surface (Figure 7b). To investigate the effect of these struts, a series of simulations is conducted with a varied displacement  $d_{xz}$  added to the magnets in the depth along the  $x$ -axis. This displacement was initiated at a value of  $b_{xz} = 1$  mm and incrementally increased up to 5 mm. The simulation results (see Table 4 and 5) show a notable reduction in the deviation areas in both the a and b regions. Less deviation is noticed for magnets in the depth with high displacement values for both regions and the majority of  $x$  values. This indicates that the incorporation of the displacement enhances the correlation between the simulation and measurement curves, thereby increasing the reliability of the model. Nevertheless, more deviation is evident between  $x = -6$  and  $x = 2$  mm in a regions and low influence at the highest thickness of the model on the left edge  $x = -18$  mm. This can be attributed to one of the following aspects of the sample: 1) In these regions, the struts in

the depth are perfectly aligned with the ones on the surface, creating perfectly lying struts in the depth under the scanned surface. This phenomenon may occur when the cells on the surface and in the depth in the surrounding region and within this area are of comparable dimensions and tilt angles. 2) The depth of the struts below the surface is relatively high. Consequently, the contribution of the magnetic field of the shifted deep struts to the signal is reduced, as they are situated at a considerable distance from the surface and the measuring probe. This may be attributed to the presence of large cells on the surface. 3) A coating discontinuity or voids in some depth regions which will be discussed in the following section.

### 3.3. Coating Discontinuity

The separation of the magnets in the simplified model represents a discontinuity in the nickel coating. Such discontinuities can be attributed to structural defects in the sample, such as missed cell struts. In addition, the pores or air gaps also represent coating

discontinuities that can be observed on the sample surface or in its depth (see Figure 1). The size, position, and distribution of these breaks or gaps exert a crucial influence on the overall magnetic flux of the sample, as well as on the overlapping nature of the magnetic field lines around these gaps.

A distinct difference between simulation and measurement curves is the presence of magnetic flux minima in the air gap regions between magnets in b regions (see Figure 4b). The magnetic field lines in these regions overlap and yield to the negative z direction opposing the magnetization direction of the magnets. This configuration results in a reduction of the calculated magnetic flux value between the magnets in the model. As it has been previously established, a displacement of the magnets in the depth leads to a slight reduction in the deviation observed in b regions.

An additional modification to the simulation model is implemented by reducing the size of the air gap, thereby aiming for a better alignment between the simulation and measurement curves. As demonstrated in Table 4, the influence from reducing the gaps between the magnets is constrained at the central region of the model at the a regions. As presented in Table 5, reducing the air gaps leads to improve the alignment of the simulation and measurements curves in b regions significantly. On the other hand, the deviation in a regions is slightly increased

Moreover, the stochastic orientation of the struts on the surface of the sample precludes the possibility of avoiding pores during the measurements.

### 3.4. Tilted Struts

The previous variation of the simplified model resulted in an enhanced convergence between the simulation and measurement curves. A relatively large deviation persists around the edges of the model at  $x = -18$  and  $x = -20, 16,$  and  $20$  mm. Previous models have operated under the assumption that all struts are parallel and have the same distance from the evaluation line. However, microscopic examination of the samples reveals a range of cell sizes and strut tilt angles. To gain a deeper insight into the impact of the tilt on the magnetic signal, a simulation of a permanent magnet with varying tilt angles around the y-axis is conducted (Figure 8). The results indicate a reduction in the magnetic flux density of  $\approx 50\%$  for a tilt angle ranging from  $0^\circ$  to  $45^\circ$  (see Figure 8a,b). A further tilt from  $45^\circ$  to  $90^\circ$  reveals a slight increase in the magnetic flux density as illustrated in Figure 8c. In each simulation, the magnetic flux is evaluated at a distance of 1 mm from the surface of the magnet.

Subsequently, the tilt is incorporated into the simplified model by rotating the magnets in the simplified model around the y-axis. The angle of the tilt is selected as  $+45^\circ/-45^\circ$  for the magnets, as illustrated in Figure 9, to examine two scenarios of tilting in a sample that normally exhibits a stochastic orientation and tilt angles.

The simulation results indicate that the maximum magnetic values of the tilted struts are slightly shifted depending on the direction of the tilt. This implies that the residual deviations can be attributed to the varying angles of tilted struts. For a regions, as it can be observed in Table 4, a significant decrease in the deviation compared to the simplified model is evident at the model edge where  $x = -18$  mm. An increase in the deviation is realized in distant regions from this edge. For b regions, a consecutive increase and decrease of the deviation are noticed along the model (Table 5). This implies that the alteration in struts tilt angle can impact the measurement signal by shifting the maximum of the magnetic field and consequently affecting the distance between the tilted struts and the measurement probe.

### 3.5. Struts Alignment on the Surface and Vertical Struts

A microscopic examination of a sample side section shows a variation in the alignment of the struts on the surface. This indicates that the distance between the scanned struts and measuring probe varies along the length of the sample. For representing this surface feature, the magnets with the center coordinates  $(-18, -10, -2, 6,$  and  $14)$  in the simplified model are moved along the z-axis by  $h_{xz}$  (Figure 10a). Three values of  $h_{xz}$  are tested, and the resulting deviation is compared with the simplified model deviation, as detailed in Table 4 and 5. Due to signal normalization, the alignment impact is influenced by the neighboring magnets and their heights. As a result, the correlation of the curves is enhanced around some a regions, especially  $x = -14$  mm at an alignment of  $h_{xz} = 0.5$  mm and  $x = 18$  mm at  $h_{xz} = 0.1$  mm. A decrease in the deviation in comparison to the simplified model is noticed in all b regions when the alignment is adjusted in some magnets in the model. The deviation decreases more at higher values of  $h_{xz}$ , particularly near the left edge of the model  $x = -16$  mm.

An additional form of cell geometry variation involves the vertical struts in a close proximity to the surface that are extending into the depth of the sample (Figure 10b). These struts are connected to the nodes situated between the struts on the surface of the sample. The investigation of their effect on the signal is carried out by introducing a set of vertical magnets in the depth and

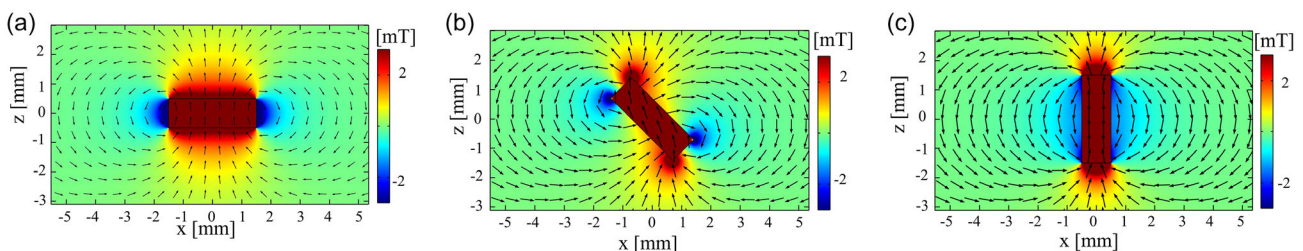


**Figure 8.** The magnetic flux density and field lines in the xz-plane for a model with a single magnet and various tilt angles. a) Tilt angle of  $0^\circ$ . b) Tilt angle of  $45^\circ$ . c) Tilt angle of  $90^\circ$ .

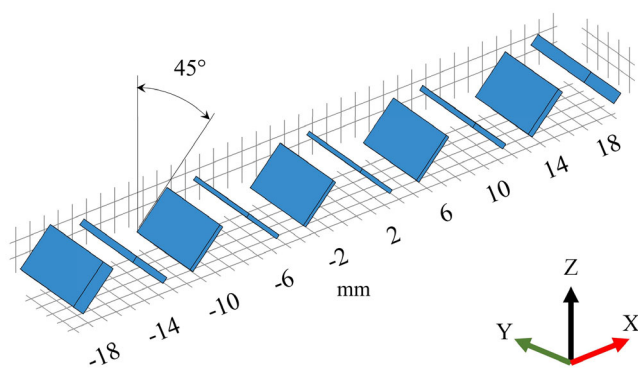


**Figure 9.** Model with tilted magnets around the  $y$ -axis in angles of  $+45^\circ$  and  $-45^\circ$ .

with an identical thickness to those on the surface of the simplified model. The added magnets are situated in the interstitial regions (gaps) between the pre-existing magnets. The distance between the added magnets and the pre-existing ones  $r_{xz}$  is varied. As demonstrated in Table 4 and 5, the incorporation of vertical magnets provide a better correlation of the curves, particularly when the magnets are situated in closer proximity to the evaluation line. The greatest impact of the additional magnets is observed on the right edge of the model ( $x = 18$  mm) for the a regions. In the b regions, the additional magnets lead to notable improvements in the correlation of the curves along the model, particularly when the vertical magnets are situated in close proximity to the evaluation line.

The results from all previous simulations are presented in Table 4 and 5. These tables present the mean values of the magnetic flux density  $B_z$  at a and b regions for a range of proximities. The mean is calculated for the magnetic flux density following a normalization to its maximum value. This is applied to the data from previous models that are created for each investigated feature, in addition to the simplified model and measurement data.

#### 4. Discussion

The mechanical properties of the coated open-cell foam depend on the coating thickness and its gradient. As it has been presented in ref. [14], the mechanical load is carried out by the

coated layer, and hence, identifying and locating inhomogeneities in the thickness is significant for accurately defining the sample properties and improving the overall manufacturing quality. The remanent magnetic field scanning of the hybrid foams<sup>[17]</sup> provides a semi-automated method for obtaining useful information about the homogeneity of the coating and the coating thickness gradient. The experimental data are validated with the simulation results of a simplified numerical model. This study applies a series of variation on the simplified model to analyze which specific geometrical feature affects the magnetic signal and analyze the magnitude of the impact of these features on the magnetic signal. The investigation is performed at varying distances from evaluation line to examine the impact of features proximity to the surface on the signal. This impact is defined by the level of correlation between the simulation and measurement curves at specific regions along them. The investigated features are revealed through a microscopic examination of five coated open-cell hybrid foam samples.

As illustrated in Table 4, the mean value of the normalized magnetic field within a regions exhibits similarities for some features. For example, the mean value of  $B_z$  at  $x = -14$  mm is  $\approx 35\%$  for adjacent cells on the surface and coating discontinuity. Furthermore, several features result in a magnetic flux density of  $\approx 75\%$  at  $x = 18$  mm as for adjacent cells in the depth and struts alignment on the surface at 0.1 mm. By calculating the deviation between the calculated and measured values, as illustrated in Figure 11a, it can be observed that the largest deviation from the measurements is present at the left edge of the model, where the value of the magnetic field and the layer thickness are higher compared to the central regions and at  $x = 14$  mm. Low deviation at  $x = 10$  mm is achieved through the utilization of the struts tilting model, adjacent magnets with a displacement and vertical magnets near the surface. At  $x = 14$  mm, less deviation is obtained by the model with magnets in the depth and a displacement distance of 5 mm. For  $x = -14$  mm, a low deviation can be achieved by adding a misalignment of 0.3 mm to the surface magnets or adding adjacent magnets in the depth with a displacement of 5 mm.

A comparison of  $d_{xz_1}$  and  $d_{xz_2}$  reveals that for this feature, the impact on the signal increases at higher displacement values around the edges of the model. The central region deviation, between  $x = -6$  and  $x = 10$  mm, is low for vertical magnets in the depth, adjacent magnets in the depth, tilted magnets, and adjacent magnets in the depth with a displacement of 1 mm.

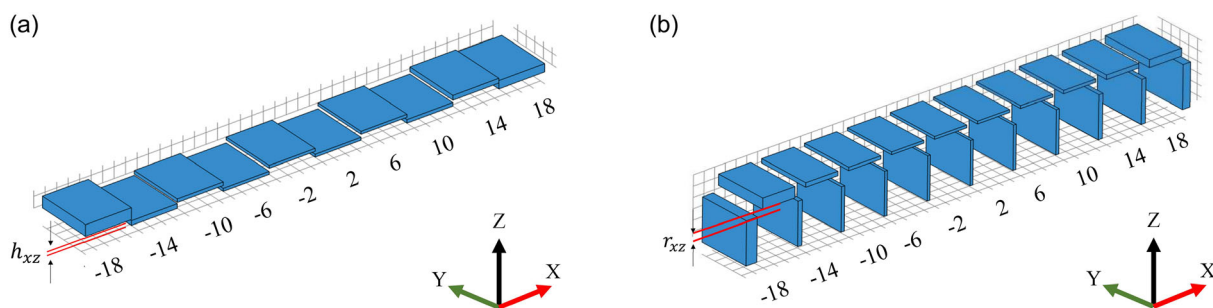


**Figure 10.** a) A model with a varied alignment of the magnets. The amount of alignment variation is referred to as  $h_{xz}$ . b) A model with additional vertical magnets in the depth. The distance between vertical and surface magnets is referred to as  $r_{xz}$ .

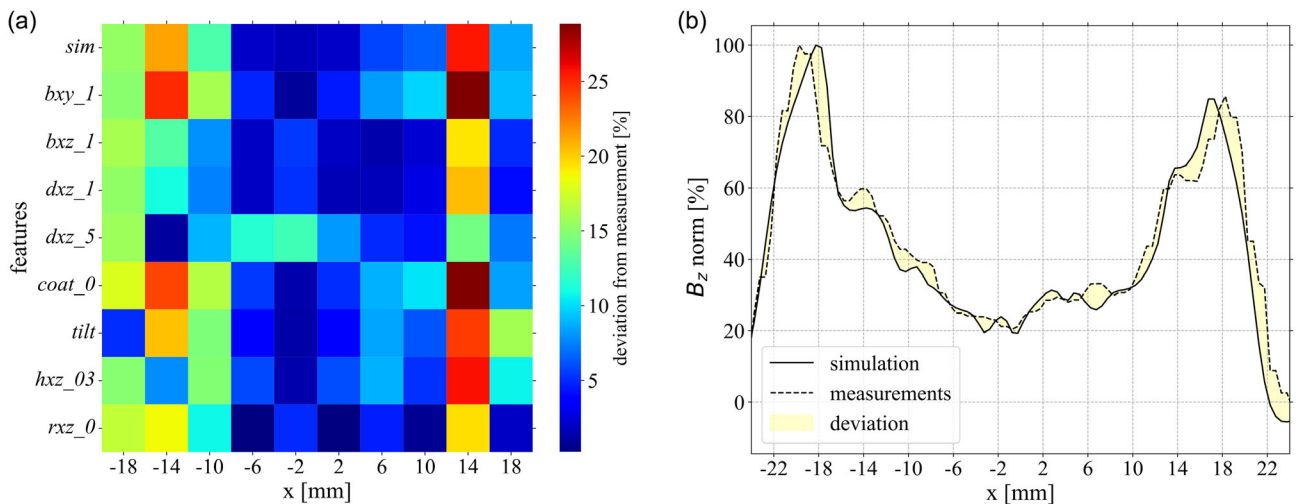


**Figure 11.** Graphical summary of selected results of the simplified model. a) Heat map of the deviation between the normalized magnetic flux density for some geometrical features and the measurement at the center of magnets (a regions). b) Normalized curves of measured values using remanent magnetic scanning and simulation empirical model with the deviation area in between.

For b regions, as given in Table 5 the model with vertical magnets in the depth at  $r_{xz} = 0$  mm exhibits the least deviation for the majority of b regions. The coating discontinuity model provides comparable  $B_z$  values to those observed in the measurement around  $x = -16, -8, -4,$  and  $0$  and the lowest deviation value for  $x = 16$  mm. Furthermore, similar to the a regions, increasing the displacement of the magnets in the depth results in enhanced alignment around the majority of  $x$  values except for  $x = -16$  and  $16$  mm. The alteration remains relatively minor for these  $x$  values. Finally, based on the results presented in Table 4 and 5, an empirical model with a combination of features with a low deviation from measurement data is created. In this model, 10 magnets of varying length are incorporated along the evaluation line, with length ranging from 5 to 2.5 mm. The magnets positioned on the edges of the model are tilted in  $\pm 10$  degrees. Furthermore, five additional vertical magnets are incorporated into the model at varying depths and in different tilt angles at  $x = -22, -12, -6, 4,$  and  $16$  mm. The combination of several features with low deviation values into one model allows a notable reduction in the deviation area between the measurement and simulation curve as shown in Figure 11b. The position of the peaks in the simulation curve around  $x = -22$  to  $-18$  and  $x = 14$  to  $18$  mm can be optimized by iteratively altering the tilt angle of edge magnets. The simulation results of the previously investigated models (see Table 4 and 5) suggest a similar influence of multiple features in some regions on the magnetic signal. Therefore, a model comprising an alternative feature combination may provide comparable results as to those observed in Figure 11b resulting in ambiguities for prediction of geometrical features. This finding has several implications for the interpretation of simulation results and, subsequently, measurement signals. Ambiguities will prevent the deduction of certain morphological features. This complicates the process of quantitatively analyzing the measured signal and distinguishing between the thickness information and all superposing geometrical features. In the future, a more extensive set of experimental

data with similar thickness profile and different geometrical features is needed to validate the simulations and provide more insights into the possibility to use magnetic scanning measurements for quantitative analysis.

## 5. Conclusion

The complexity of the interplay between the selected geometrical features influence on the magnetic characterization of hybrid foams was shown with the variation of a simplified numerical model. Several independent features showed similar effects on the magnetic field, yielding ambiguities in the interpretation. According to the simulations, attributing the signal change in some regions to a specific geometrical feature including the local thickness variation is therefore not possible without an additional validation method. In order to experimentally quantify the local thickness of a coating using the magnetic signal from remanent field scanning, it is necessary to examine the scanned sample microscopically. Based on these information, the simplified model can be modified and assist in quantifying the underlying thickness distribution of samples. In summary, the remanent magnetic scanning method and the simplified model still provide a qualitative and fast approach for the estimation of the thickness gradients along the sample assuming the geometrical features of individual samples are relatively homogeneous. In the future, to extend this method and enable comparison between different samples, more experimental data and a systematic study of overlapping features are needed.

## Acknowledgements

This work was supported by a Fraunhofer Internal Program under the grant no. Attract 025-601314 awarded to S.C.L.F. The authors gratefully acknowledge the DFG (German Science Foundation – Deutsche

Forschungsgemeinschaft) through the grant number JU 2962/8-1 for partially funding this work.

Open Access funding enabled and organized by Projekt DEAL.

## Conflict of Interest

The authors declare no conflict of interest.

## Author Contributions

**Bashar Ibrahim:** conceptualization (equal); data curation (lead); investigation (lead); methodology (lead); validation (lead); visualization (lead); writing—original draft (lead); writing—review and editing (equal). **Michael M. Becker:** conceptualization (equal); methodology (supporting); writing—review and editing (supporting). **Sarah C. L. Fischer:** funding acquisition (equal); project administration (lead); supervision (lead); writing—review and editing (equal). **Anne Jung:** funding acquisition (equal); project administration (supporting). **Francesco Kunz:** methodology (supporting); writing—review and editing (supporting).

## Data Availability Statement

The data that support the findings of this study are available from the corresponding author upon reasonable request.

## Keywords

coating thickness, magnetic flux, open-cell, simplified model, struts

Received: August 30, 2024

Revised: April 7, 2025

Published online:

- [1] J. Banhart, G. S. Vinod-Kumar, P. H. Kamm, T. R. Neu, F. García-Moreno, *Ciência Tecnologia dos Materiais* **2016**, *28*, 1.
- [2] L. Philippe Lefebvre, J. Banhart, D. C. Dunand, *Adv. Eng. Mater.* **2008**, *10*, 775.
- [3] M. F. Ashby, A. G. Evans, N. A. Fleck, L. J. Gibson, J. W. Hutchinson, H. N. G. Wadley, Metal Foams, <https://doi.org/10.1016/B978-0-7506-7219-1.X5000-4>
- [4] S. Rashidi, M. Hossein Kashefi, K. Chun Kim, O. Samimi-Abiane, *Appl. Energy* **2019**, *243*, 206.

- [5] W. Yang, S. Yang, W. Sun, G. Sun, Q. Xin, *Electrochim. Acta* **2006**, *52*, 9.
- [6] J. Banhart, *Prog. Mater. Sci.* **2001**, *46*, 559. [https://doi.org/10.1016/S0079-6425\(00\)00002-5](https://doi.org/10.1016/S0079-6425(00)00002-5)
- [7] M. Reinfried, G. Stephani, F. Luthardt, J. Adler, M. John, A. Kromholz, *Adv. Eng. Mater.* **2011**, *13*, 1031.
- [8] A. Hassan, I. Abdullah Alnaser, *ACS Omega* **2024**, *9*, 6280.
- [9] J. Liu, Y. Li, X. Gao, P. Liu, L. Kong, *Int. J. Crashworthiness* **2015**, *20*, 325.
- [10] A. Jung, S. Diebels, *Adv. Eng. Mater.* **2016**, *18*, 532.
- [11] A. Jung, Z. Chen, J. Schmauch, C. Motz, S. Diebels, *Acta Mater.* **2016**, *102*, 38.
- [12] A. Jung, S. Brönder, S. Diebels, M. Schmidt, S. Seelecke, *Mater. Des.* **2018**, *160*, 363.
- [13] F. Kunz, A. Jung, *Adv. Eng. Mater.* **2022**, *24*, 2200262.
- [14] S. Heinze, T. Bleistein, A. Düster, S. Diebels, A. Jung, *J. Appl. Math. Mech.* **2018**, *98*, 682.
- [15] A. Jung, T. Grammes, S. Diebels, *Arch. Appl. Mech.* **2015**, *85*, 1147.
- [16] A. Sutygina, *Manufacturing and characterization of open-cell metal foams with high strut porosity. Dissertation (Dr.-Ing.), Otto-von-Guericke-University Magdeburg* **2022**.
- [17] F. Kunz, B. Ibrahim, M. Becker, H. Gao, S. C. L. Fischer, A. Jung, *Adv. Eng. Mater.* **2024**, *26*, 2302172.
- [18] Comsol, AC/DC Module Application Library, <https://doc.comsol.com/5.3/doc/com.comsol.help.acdc/ACDCApplicationLibraryManual.pdf>. (accessed: April 2024).
- [19] Comsol, COMSOL Multiphysics Application Library, [https://doc.comsol.com/5.3/doc/com.comsol.help.comsol/COMSOL\\_ApplicationLibraryManual.pdf](https://doc.comsol.com/5.3/doc/com.comsol.help.comsol/COMSOL_ApplicationLibraryManual.pdf). (accessed: April 2024).
- [20] Comsol Documentation, Infinite Element Domain, [https://doc.comsol.com/5.5/doc/com.comsol.help.comsol/comsol\\_ref\\_definitions.12.116.html](https://doc.comsol.com/5.5/doc/com.comsol.help.comsol/comsol_ref_definitions.12.116.html). (accessed: April 2024).
- [21] Comsol Blog, Understanding and Changing the Element Order, <https://www.comsol.com/support/learning-center/article/Understanding-and-Changing-the-Element-Order-53461>. (accessed: April 2024).
- [22] Comsol, COMSOL Multiphysics Reference Manual, [https://doc.comsol.com/5.5/doc/com.comsol.help.comsol/COMSOL\\_ReferenceManual.pdf](https://doc.comsol.com/5.5/doc/com.comsol.help.comsol/COMSOL_ReferenceManual.pdf). (accessed: May 2024).
- [23] Comsol Documentation, Fully Coupled, [https://doc.comsol.com/5.5/doc/com.comsol.help.comsol/comsol\\_ref\\_solver.27.149.html](https://doc.comsol.com/5.5/doc/com.comsol.help.comsol/comsol_ref_solver.27.149.html). (accessed: May 2024).
- [24] M. Pelanconi, E. Rezaei, A. Ortona, *J. Ceram. Soc. Jpn.* **2020**, *128*, 595.
- [25] A. Jung, D. Klis, F. Goldschmidt, *J. Magn. Magn. Mater.* **2015**, *378*, 178.
- [26] J. Storm, M. Abendroth, M. Kuna, *Mech. Mater.* **2019**, *137*, 103145.